THE INFLUENCE OF SPARK PLASMA SINTERING PARAMETERS ON THE PHYSICAL PROPERTIES OF CoCrMoNbTi Bio-HEA

Alina Elena BOLOLOI[1], Ciprian Alexandru MANEA[2]*, Iulian Vasile ANTONIAC[3], Robert Viorel BOLOLOI[4], Vasile Dănuţ COJOCARU[5], Dorinel TĂLPEANU[6], Delia PĂTROI[7], Laura Elena GEAMBAZU[8]

The paper presents the influence of the sintering temperature parameter on the physical properties of CoCrMoNbTi high entropy alloy intended for biomedical applications. CoCrMoNbTi HEA metallic powder preparation method was disseminated previously. The alloy was consolidated by spark plasma sintering in order to produce bulk materials which could be further processed. The produced samples were analyzed monitoring the structure, apparent density and hardness modifications. The microstructural and chemical analyses results indicated a good elemental distribution and compaction, with no contamination present. Hardness and density measurements indicated a direct proportional increase with the temperature.

Keywords: HEA, SPS, Bio-HEA, HEA sintering.

1. Introduction

Biomedical high entropy alloys, also known as Bio-HEA, are a new class of materials designed for medical purposes due to their excellent biocompatibility and mechanical properties, with application for medical devices. The advantages

[1] PhDs., Material Science and Engineering Faculty, National University of Science and Technology POLITEHNICA Bucharest, Romania, e-mail: alina_elena.boarna@upb.ro
[2] PhD. Eng., National Institute for R&D in Electrical Engineering ICPE-CA Bucharest, Romania, email: ciprian.manea@icpe-ca.ro **correspondent author*
[3] Prof., Material Science and Engineering Faculty, National University of Science and Technology POLITEHNICA Bucharest, Romania, e-mail: antoniac.iulian@gmail.com
[4] PhD. Eng., Material Science and Engineering Faculty, National University of Science and Technology POLITEHNICA Bucharest, Romania, e-mail: robert.bololoi@upb.ro
[5] Prof., Material Science and Engineering Faculty, National University of Science and Technology POLITEHNICA Bucharest, Romania, e-mail: dan.cojocaru@upb.ro
[6] PhD. Eng., National Institute for R&D in Electrical Engineering ICPE-CA Bucharest, Romania, email: dorinel.taleanu@icpe-ca
[7] PhD. Eng., National Institute for R&D in Electrical Engineering ICPE-CA Bucharest, Romania, email: delia.patroi@icpe-ca.ro
[8] PhD. Eng., National Institute for R&D in Electrical Engineering ICPE-CA Bucharest, Romania, email: laura.geambazu@icpe-ca.ro

are brought by the possibility of tailoring the materials for implants based on factors as age, sex, activity levels, preexisting conditions of the patient, but also the possibility of aiding the healing process when using them as implants in or near a bone fracture to facilitate healing or to compensate for missing or lost bone tissue [1]. A critical aspect regarding the Bio-HEA properties is represented by the compositional elements' selection, where the principal biocompatible elements used are Ti, Zr, Hf, Nb, Ta, V, Mo and W. The elements do not cause secondary harmful effects on the tissue adjacent to the implant area or they are considered to be safe to be used because they are in the safety interval of adverse effects that could be caused to the body during the implantation period [1].

In recent years, the high entropy alloys, also known as HEAs, became one of the most promising materials for the biomedical field mostly due to their biological safety, high resistance to corrosion and wear and excellent mechanical properties. Due to the dual effect of the HEAs, they could be tailored based on final properties, having the capacity of producing materials with a larger specter of applicability in numerous domains [1]. The specific effects of the HEAs known as high-entropy effect, slow diffusion effect, lattice disorder effect and cocktail effect [1], made them a desirable new alloy in multiple research studies due to the possibility of producing materials tailored for particular applications [2-7].

Belonging to the class of high entropy alloys, the Bio-HEA materials have the same design concept. Due to the large number of possible component elements and due to the high content of each component, the chemical synergy and the complex physical properties between the different alloying elements will contribute in a great proportion improving the microstructure and mechanical properties of the resulting alloys [8-10].

The first steps into producing a biocompatible material consisted in developing the CoCrMoNbTi HEA from raw pure materials by solid state processing in a planetary ball mill, where the microstructural and chemical characteristics were studied [11]. The HEA metallic powder mechanical alloying process was disseminated by the authors [11]. The results indicated that a high degree of alloying was obtained after 30 h, with a good distribution of elements and no contamination. It was also observed that dual BCC1 and BCC2 (body centered cubic) phases were formed along TVC (tetragonal) phases in the HEA metallic powder indicating low ductility but with relatively high fracture strength [12]. The present paper investigates the influence of the spark plasma sintering (SPS) parameters on the powder materials chemical and physical properties, with the end goal of establishing the most suitable parameters of the consolidation process for the studied case. SPS method was selected for this experimentation due to the high capabilities of densifying by pressing and heating the powder materials [13] in a short time (approx. 30 min), with controlled heating and cooling rate resulting density values close to the calculated theoretical ones. Other

advantages of this method consist of a low oxidation degree due to the controlled atmosphere, low pressing force, but also low porosity and defects. The consolidated HEA samples were evaluated in terms of microstructural and chemical changes, hardness and density and the results are presented.

2. Materials and Methods

In order to produce the consolidated SPS samples, CoCrMoNbTi high entropy alloy produced by mechanical alloying in a planetary ball mill was used. The powder mixture was alloyed for 30 h with 2 wt% process control agent (N-Heptane) with a 10:1 ball to powder ratio and 300 RPM, with an average particle size of 45.12 μm, the results being disseminated previously [11].

The sintering process was produced by SPS in vacuum, with HP D25 FCT Systeme GmbH, Effelder-Rauenstein, Germany equipment by using a high-density graphite die, lined with graphite foil. Graphite felt was used to cover the die assembly during the process in order to avoid temperature losses. The sintering curves for each experimentation are presented in Fig. 1.

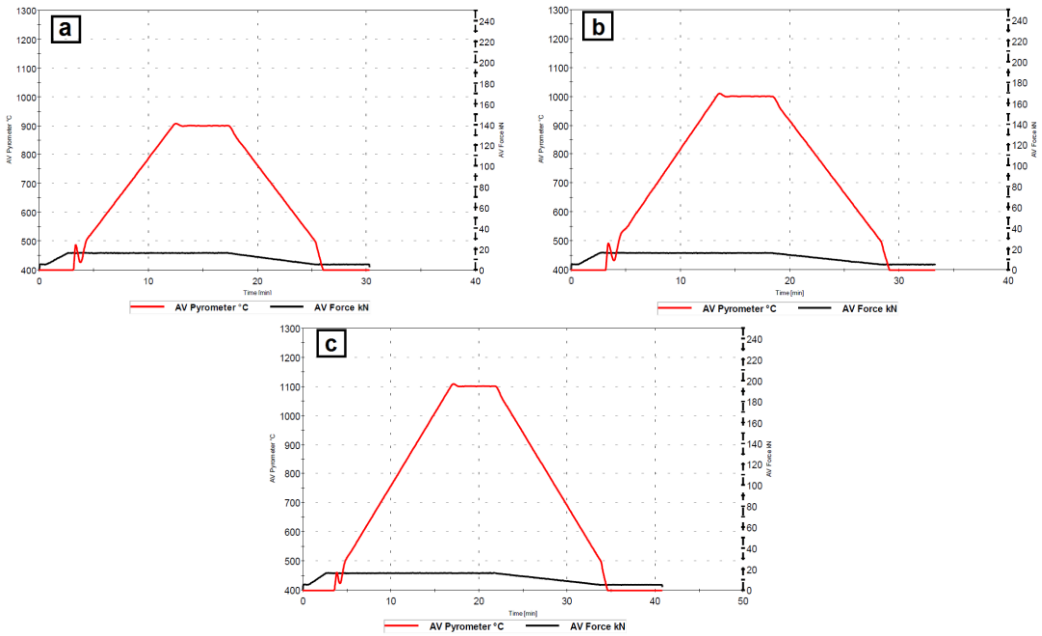

Fig. 1. Sintering curve graphs for the samples consolidated by SPS at a) 900°C, b) 1000°C and c)1100°C

In order to establish the SPS process parameters influence, three different sintering temperatures were used, namely 900°C, 1000°C and 1100°C, a graphite die with a diameter of 20 mm, a pressing force of 16 kN, a heating/cooling rate of 50°C/min and a dwell time of 5 min. Henceforth, the produced trial samples will

be referred as P1 (sintered at 900°C), P2 (sintered at 1000°C) and P3 (sintered at 1100°C).

Microstructural and chemical composition analysis were performed with Tescan Vega II-XMU SEM (Tescan Group, Kohoutovice, Czech Republic) coupled with a Bruker xFlash 6/30 EDS detector (Bruker, Cordoba, Argentina) equipment. The equipment was also used to perform elemental mapping analysis in order to observe the distribution of the constituent chemical elements, X-ray diffraction analysis were carried out by using a D8-Discover diffractometer, Bruker, Germany, Goebel mirror and 1D LynxEye detector (Bruker AXS, Germany) on the secondary side, with Cu primary radiation (λ = 1.540598 Å). The diffractograms were obtained by using an angular increment of 0.04°, at a scanning speed of 1 s/step. The crystallographic phases were identified by using ICDD PDF 2 Release 2022 database, where the structures were similar to the following indexed files PDF01-086-8528, PDF 01-087-4196, PDF 01-086-9398, PDF 01-071-7326, PDF 01-074-7072, PDF 01-086-4055, PDF 03-065-7486 for P1, PDF 01-081-4924, PDF 00-042-1120, PDF 03-065-5102, PDF 01-078-8914, PDF 03-066-0004, PDF 03-065-7479, PDF 01-078-8915, PDF 01-071-7570 for P2 and PDF 01-078-8914, PDF 03-065-7442, PDF 01-086-7232, PDF 01-071-7570, PDF 00-029-0490, PDF 00-042-1211 for P3. Hardness tests were performed with FM 700 (Future Tech, Japan) hardness tester using the load of 1 kgf for 15 sec and apparent density of the compacted samples was measured by using an analytical hydrostatic balance, type XS204M, Mettler Toledo, USA, in order to determine the compaction degree and the results are presented.

3. Results and Discussions

The SPS processed samples analyses results indicated the microstructural compaction degree and are presented in Fig. 2 a-c. As it could be observed, pores were present on the analyzed surfaces indicating a possible low mechanical resistance, but the pores size and number decreased proportionally with the temperature parameter increment.

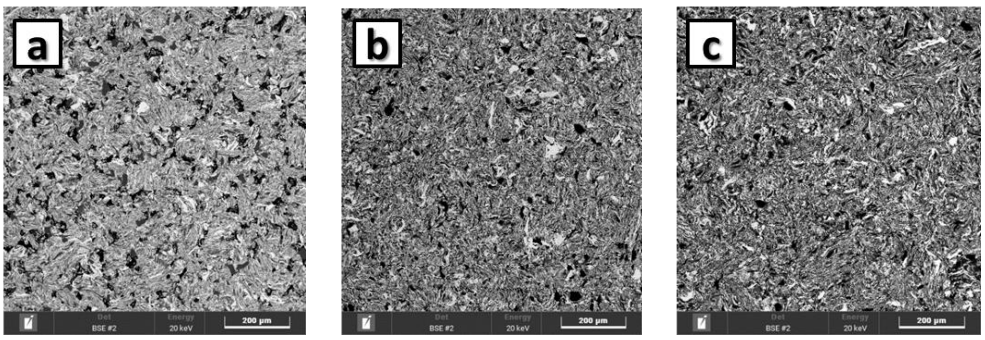

Fig.2. SEM microstructural analyses for a) P1, b) P2 and c) P3

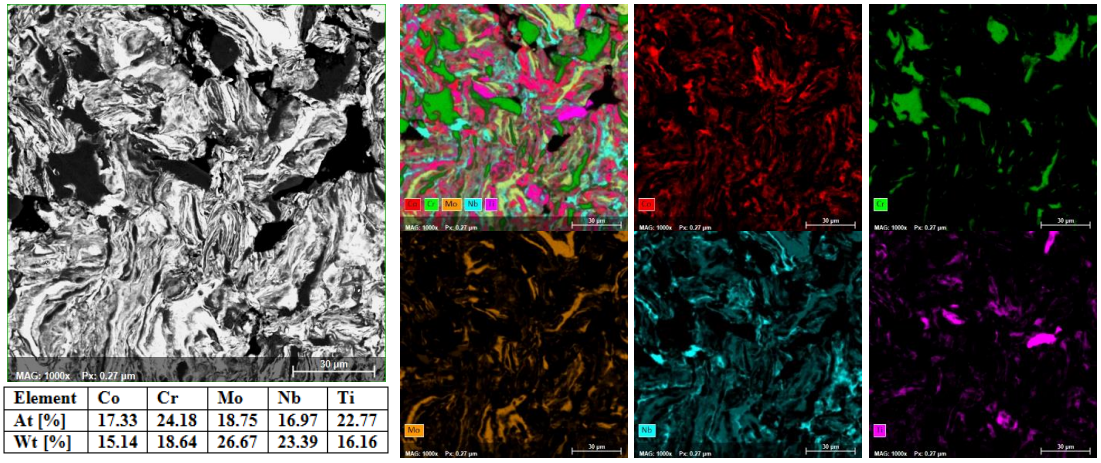

Element	Co	Cr	Mo	Nb	Ti
At [%]	17.33	24.18	18.75	16.97	22.77
Wt [%]	15.14	18.64	26.67	23.39	16.16

Fig. 3. Mapping and chemical analyses for sample P1

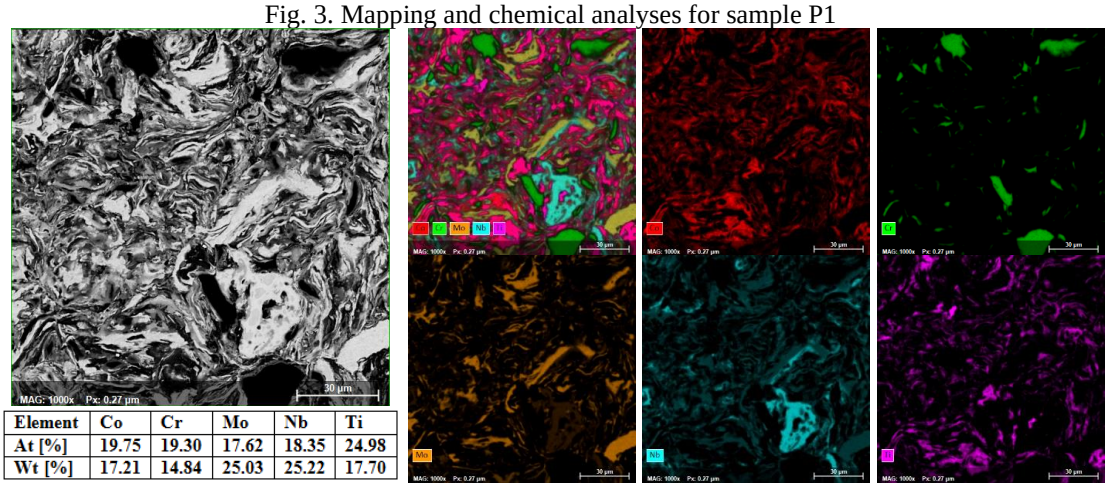

Element	Co	Cr	Mo	Nb	Ti
At [%]	19.75	19.30	17.62	18.35	24.98
Wt [%]	17.21	14.84	25.03	25.22	17.70

Fig. 4. Mapping and chemical analyses for sample P2

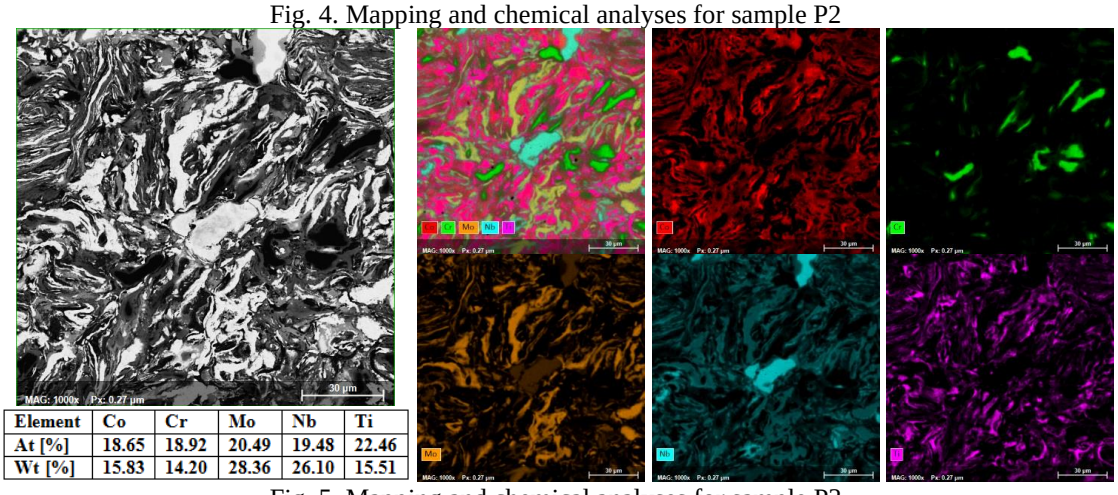

Element	Co	Cr	Mo	Nb	Ti
At [%]	18.65	18.92	20.49	19.48	22.46
Wt [%]	15.83	14.20	28.36	26.10	15.51

Fig. 5. Mapping and chemical analyses for sample P3

Figs. 3-5 present the chemical composition analysis and the elemental distribution of the analyzed samples. As observed, the elemental composition is confirmed with no contamination involved during the production process and with a near equiatomic ratio for sample P3. The Oxygen and Carbon content were taken into consideration as possible traces, but the content levels were under the instrumental detection limit. Due to the average particle size of 45.12 μm of the powder mixture (mentioned in section 2 Materials and methods) the mapping analyses reveal a high alloying degree for the samples, but with a common patchy Cr distribution, revealing the necessity of further mechanical alloying parameters adjustment. As previously stated, micro-pores are visible, but reduced in size when analyzing sample P3, indicating a possible improvement of the mechanical properties.

From the XRD comparative analyses patterns presented in Fig. 6, it was observed that for P1 and P2, the highest peak intensity was identified at the 2θ angular position of 40.5°, whereas for P3 was identified at the 2θ angular position of 41.0° along with a high intensity phase identified at 39.5°. For all the samples analyzed, BCC was identified as a major crystalline phase with particular trigonal (T) symmetry with hexagonal axis for P1, orthorhombic (O), hexagonal (HCP) and TVC major phases for P2 and P3. Also, a low crystallinity degree face centered cubic (FCC) phase was identified for all samples.

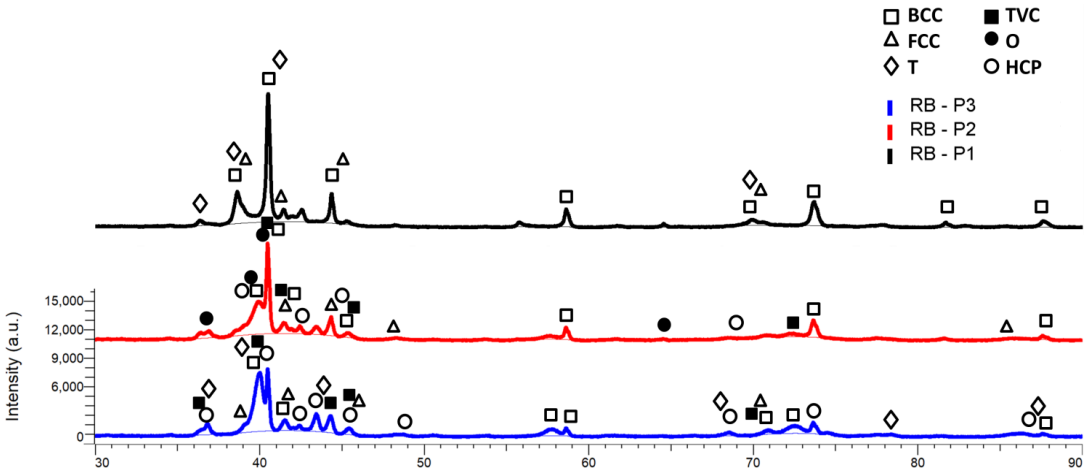

Fig. 6. Comparative XRD analysis for samples P1, P2 and P3

Qualitative phase identification of the principal peaks indicates the presence of the alloying components and confirms both the composition and the increased alloying degree of the HEA.

When analyzing the sintering evolution via the comparative XRD results, it could be observed that the peak initially observed at angular position 2θ of 38.5°, assigned to BCC single-phase, shifted towards higher angular position

(suggesting changes in lattice parameters related to the local stoichiometric composition) and increased in intensity when the sample was sintered at 1100° C. It could also be observed a peak broadening indicating the evolution of alloying degree, but the tendencies suggest the need of a higher temperature during the sintering process.

For *sample P1*, Mo, Ti, Nb, Cr and CoMo were identified as mainly single elemental or combined crystalline phases at angular position 2θ of 40.5°, highest intensity peak, 44.5°, 38.5°, 55.5°, 58.5, 70.0°, 74.0°, 81.5°, 89.0° and minor phases with a BCC crystalline structure. A particular trigonal structure with hexagonal axis of CoNb was identified at the angular positions 2θ of 36.5°, 40.2°, 42.5°, 45.1° and 70° indicating a low mechanical resistance. According to literature [14-16], it was observed that an optimal resistance and ductility ratio could be induced when the HCP and BCC phases coexist in the crystalline structure, which could suggest similar properties of the current studied material.

The presence of the FCC minor single phase of CoTi was identified at the 2θ angular positions of 39.0°, 41.2°, 45.2°, 70.5° indicating possible properties as increased tensile strength and increased ductility in the alloy [14,17]. The observation correlates with the ductile nature of Ti found in this crystallographic structure. The valence electron concentration (VEC), that yielded a value of 6 [11], indicate de formation of a majority of BCC phase with the possibility of FCC phase formation, as confirmed by the XRD. The presence of the phases indicates high ductility (FCC) and fracture strength (BCC) of the final alloy.

Sample P2 analysis highlighted the formation of BCC phase at the 2θ angular positions of 39.5°, 41.0°, 41.5°, 45.5°, 58.5°, 73.0°, 74.0° and 88.0° with an abundance of Mo, MoNb, CrMoNb, FCC at the 2θ angular positions of 41.5°, 45.0°, 48.0° and 86.0° with a binary system of Co-Ti, trigonal phase at the 2θ angular positions 32.0°, 34.0°, 39.0°, 41.0°, 42.0°, 44.0°, 45.0°, 72.0° and 75.0° with a binary system of Co-Mo, HCP phase at the 2θ angular positions 39.5°, 42.0°, 43.0°, 44.0°, 45.5°, 68.5° with an abundance of CrCoNb. Distinctively for P2 when compared with P1 and P3, an orthorhombic phase was identified with an abundance of NbTi at the 2θ angular positions of 37.0°, 39.0°, 41.0° and 64.5°. According to literature [18], when Ti2AlNb based alloys were analyzed by XRD, it was observed that the orthorhombic phase is the principal hardening phase of the material. After annealing the Ti40Nb30Hf15Al15 sample at 600°C [19] the authors noticed a substantial resistance growth, possible due to orthorhombic phase precipitation. For the present case, high fracture strength and low ductility [20] was taken into consideration due to the major BCC phase formation according to the VEC value [11, 12].

For *sample P3*, it was revealed the presence of BCC phase with an abundance of Mo and CoMoNb at the angular positions 2θ of 40.0°, 40.5°, 58.0°, 72.5°, 86.5° and 87.5°, HCP phase with an abundance of CrCoNb at 2θ angular

positions of 37°, 41°, 42.5°, 44.2°, 45.5°, 48.5°, 50.5°, 71.0° and 87.0°, FCC phase with an abundance of CoTi at 2θ angular positions of 39.0°, 41.5°, 44.5°, 70.5°, the presence of a trigonal structure with hexagonal axis, similar to the P1 sample case, was identified at 2θ angular positions of 37.0°, 40.0°, 43.5°, 44.5°, 48.5°, 68.0°, 77.5° and 87.5° with an abundance of CoNb, but also the TVC phase with an abundance of CoMo at 2θ angular positions of 37.0°,41.5°, 43.5°, 44.5°, 45.5°, 70.0° and 71.5°.

In order to observe the SPS parameters effect on the porosity and densification degree, the compacted samples were tested by hydrostatic method. Hardness testing was also performed on the surface of the bulk samples in order to observe the SPS temperature influence. For each sample, 5 measurements were performed in accordance to ISO 6507-1:2023 – Vickers hardness test and the mean values were calculated. The results are presented in table 1.

Table 1

Hardness measurements and hydrostatic test results for the SPS sintered samples

Sample	SPS Temperature (°C)	Vickers Average Hardness (HV)	Apparent Density (g/cm3)	Densification Degree (%)	Apparent Porosity (%)
P1	900	507.40	6.552	84.11	15.89
P2	1000	664.37	7.394	94.91	5.08
P3	1100	823.63	7.710	98.97	1.03

The highest hardness value of 823.63 HV was obtained for sample P3, which was sintered at 1100°C. The outcome was to be expected and it is in agreement the VEC value and the XRD identified major BCC single phase.

The hydrostatic density indicated that sample P3 has a densification degree of 98.97% with an apparent density of 7.710 g/cm^3, where the theoretical density of the equiatomic CoCrMoNbTi high entropy alloy is 7.79 g/cm^3. A high apparent porosity was observed for sample P1 of 15.89% in good agreement with the observed aspects from the microstructural characterization.

4. Conclusions

CoCrMoNbTi high entropy alloy metallic powder was sintered via SPS technique at different temperatures (900°C, 1000°C, 1100°C) and the results indicated that with the temperature increment, the structural pores size and distribution are reduced, indicating an improvement of the mechanical resistance.

The EDS and elemental mapping indicated a high alloying degree with a good elemental distribution and no contamination. The chemical composition of the HEA is confirmed, although Oxygen and Carbon were taken into consideration as possible traces, these could not be confirmed by the used equipment.

The XRD analyses results indicated a major BCC phase for all tested samples along with T, O, HCP, TVC, but also minor FCC phase resulting in properties as high fracture strength and possible ductility according to the theory [12].

Hardness measurements presented a higher HV value for the sample sintered at 1100°C when compared to the samples sintered at 900°C and 1000°C, being in correlation with the 98.97% densification degree resulted from the hydrostatic method tests.

The results indicate that sample P3 is a good candidate for wear resistance applications.

R E F E R E N C E S

[1] *J.Feng, Y.Tang, J.Liu, P.Zhang, C.Liu and L.Wang*, "Bio-high entropy alloys: Progress, challenges, and opportunities" Front. Bioeng. Biotechnol. **vol.10**, no.977282, 2022.

[2] *R.V.Bololoi; M. Sohaciu; V.S. Serban-Tanase, F.Miculescu and I.Csaki*, "AlCrFeNiTi high entropy alloy produced by solid state processing" U.P.B. Sci. Bull., **vol. 83**, 2021, pp. 265–274.

[3] *A.Olejarz, W.Y.Huo, M.Zielinski, R.Diduszko, E.Wyszkowska, A.Kosinska, D.Kalita, I.Józwik, M. Chmielewski, F. Fang, et al.* "Microstructure and mechanical properties of mechanically-alloyed CoCrFeNi high-entropy alloys using low ball-to-powder ratio", J. Alloys Compd., **vol. 938**, no. 168196, 2023.

[4] *H.Kotan, M. Tekin, A. Bayatlı, K.G. Bayrak, M. Kocabas and E. Ayas*, " Effect of in-situ formed oxide and carbide phases on microstructure and corrosion behavior of Zr/Y doped CoCrFeNi high entropy alloys prepared by mechanical alloying and spark plasma sintering" Intermetallics, **vol. 162**, no. 107998, 2023.

[5] *K.Li, Y. Zhai, M. Lai, M. Song, S. Zou, G. Huang, K. Yaqoob, Z.Wang and N. Zhang*, "Corrosion of Eutectic High-Entropy Alloys: A Review", Crystals, **vol. 13**, no. 1231, 2023.

[6] *N.Hua, W. Wang, Q.Wang, Y. Ye, S. Lin, L. Zhang, Q. Guo, J. Brechtl and P.K. Liaw* "Mechanical, corrosion, and wear properties of biomedical Ti–Zr–Nb–Ta–Mo high entropy alloys" J. Alloys Compd., **vol. 861**, no.157997, 2021.

[7] *C.A. Naciu, M. Nicolae, C.A. Manea, L.E. Geambazu, and C. Morari*, "High Entropy Alloys with Shielding Properties for Aggressive Media." UPB Sci. Bull. **vol. 85**, 2023, pp.179–184.

[8] *D.Castro, P. Jaeger, A.C. Baptista and J.P.Oliveira*, "An Overview of High-Entropy Alloys as Biomaterials", Metals, **vol. 11**, no. 648, 2021.

[9] *M.Todai, T.Nagase, T.Hori, A.Matsugaki, A.Sekita and T.Nakano*, "Novel TiNbTaZrMo high-entropy alloys for metallic biomaterials", Scripta Materialia, **vol. 129**, 2017, pp. 65–68.

[10] *J.Shittu, M.Pole, I.Cockerill, M.Sadeghilaridjani, L.V.K. Reddy, G.Manivasagam, H. Singh, H. S. Grewal, H.S.Arora, and S.Mukherjee*, "Biocompatible High Entropy Alloys with Excellent Degradation Resistance in a Simulated Physiological Environment", ACS Appl. Bio Mater., **vol. 3**, no. 12, 2020, pp. 8890–8900.

[11] *A.E.Bololoi, L.E. Geambazu, I.V.Antoniac, R.V. Bololoi, C.A. Manea, V.D. Cojocaru, and D.Pătroi,* "Solid-State Processing of CoCrMoNbTi High-Entropy Alloy for Biomedical Applications", Materials, **vol. 16**, no. 6520, 2023.

[12] *S. Guo and C.T.Liu*,," Phase stability in high entropy alloys: Formation of solid-solution phase or amorphous phase", Prog. Nat. Sci. Mater. Int., **vol. 21**, 2011, pp. 433−446.

[13] *O.Guillon, J. Gonzalez-Julian, B. Dargatz, T.Kessel, G.Schierning, J.Räthel and M.Herrmann*, "Field-assisted sintering technology / spark plasma sintering: mechanisms, materials, and technology developments", Advanced Engineering Materials, **vol. 16**, no. 7, 2014, pp. 830-849

[14] *C.A.Manea, L.E. Geambazu, D.Talpeanu, V.Marinescu, G.B.Sbârcea, D. Patroi, R.M. Udrea, M.V. Lungu and M. Lucaci*, " CoxCrFeNiTi High-Entropy Alloys Prepared via Mechanical Alloying and Spark Plasma Sintering for Magnetron Sputtering Coatings", Materials, **vol. 16**, no. 6386, 2023.

[15] *M.Peters, J. Hemptenmacher, J. Kumpfert and C. Leyens*, "Structure and properties of titanium and titanium alloys. In Titanium and Titanium Alloys", Leyens, C., Peters, M., Eds. Wiley-VCH Verlag GmbH & Co. KGaA:Weinheim, Germany, 2005, pp. 1–36.

[16] *L.Rogal, Y. Ikedab, M. Lai, F. Körmannb, A. Kalinowska and B. Grabowski*, "Design of a dual-phase hcp-bcc high entropy alloy strengthened by ω nanoprecipitates in the Sc-Ti-Zr-Hf-Re system", Mater. Des., **vol. 192**, no.108716, 2020.

[17] *D.Chung, H. Kwon, C. Eze, W. Kim, Y. Na*, "Influence of Ti Addition on the Strengthening and Toughening Effect in CoCrFeNiTix Multi Principal Element Alloys", Metals, **vol.11**, no. 1511, 2021.

[18] *C.J. Boehlert*, "Part III. The tensile behavior of Ti-Al-Nb O Bcc orthorhombic alloys", Metall. Mater. Trans. A., **vol. 32**, 2001, pp. 1977-1988

[19] *N. Yurchenko, E. Panina, M. Tikhonovsky, G. Salishchev, S. Zherebtsov, N. Stepanov*, "A new refractory Ti-Nb-Hf-Al high entropy alloy strengthened by orthorhombic phase particles", International Journal of Refractory Metals and Hard Materials, **vol. 92**, no. 105322, 2020.

[20] *T. Zhang, R.D. Zhao, F.F. Wu, S.B. Lin, S.S. Jiang, Y.J. Huang, S.H. Chen and J. Eckert*, "Transformation-enhanced strength and ductility in a FeCoCrNiMn dual phase high-entropy alloy", Materials Science and Engineering: A, **vol. 780**, no. 139182, 2020.